The near-infrared (1.30–1.70 μm) absorption spectrum of methane down to 77 K†

Samir Kassi,[a] Bo Gao,[ab] Daniele Romanini[a] and Alain Campargue*[a]

Received 9th April 2008, Accepted 13th May 2008
First published as an Advance Article on the web 19th June 2008
DOI: 10.1039/b805947k

The high resolution absorption spectrum of methane has been recorded at liquid nitrogen temperature by direct absorption spectroscopy between 1.30 and 1.70 μm (5850–7700 cm^{-1}) using a newly developed cryogenic cell and a series of DFB diode lasers. The investigated spectral range includes part of the tetradecad and the full icosad regions for which only very partial theoretical analysis are available. The analysis of the low temperature spectrum will benefit from the reduction of the rotational congestion and from the narrowing by a factor of 2 of the Doppler linewidth allowing the resolution of a number of multiplets. Moreover, the energy value and rotational assignment of the angular momentum J of the lower state of a given transition can be obtained from the temperature variation of its line intensity. This procedure is illustrated in selected spectral regions by a continuous monitoring of the spectrum during the cell cool-down to 77 K, the temperature value being calculated at each instant from the measured Doppler linewidth. A short movie showing the considerable change of a spectrum during cool-down is attached as Supplementary Material.† The method applied to a 30 cm^{-1} section of the tetradecad spectrum around 6110 cm^{-1} has allowed an unambiguous determination of the J values of part of the observed transitions.

1. Introduction

Despite many years of experimental and theoretical efforts (see, for instance, ref. 1), the considerable complexity and congestion of the near-infrared absorption spectrum of methane have hampered a satisfactory modeling above 6000 cm^{-1}. Line-by-line analysis, which is based on the expansion of an effective Hamiltonian and dipole moment, is not yet able to provide reliable models over the near-infrared range and in the CH_4 transparency windows. This issue continues to be a current research topic, in particular because the quality of the spectrum analysis of the giant outer planets and in particular of Saturn's satellite Titan, demands simulating the methane absorption spectrum for the experimental conditions existing on these planets.

Empirical line-by-line spectroscopic parameters as included in HITRAN[2] or GEISA[3] are then far from fulfilling the needs in the case of methane. For instance, above 5000 cm^{-1}, the HITRAN database provides empirical line parameters which were obtained at room temperature by high resolution Fourier transform spectroscopy (FTS) with path lengths of up to 433 m.[4] In absence of rovibrational assignments or at least of the knowledge of the energy of the transitions lower levels, line intensities cannot be extrapolated at different temperatures which makes the current HITRAN line list of limited use in planetology.

On the other hand, direct sample cooling is the simplest experimental way to reduce the spectral congestion and simplify the rovibrational analysis. Absorption spectra of methane cooled down to 77 K using cooled cells could already be investigated in several spectral regions,[5–12] thanks to the important available vapor pressure (~10 Torr). Further cooling was also achieved by means of supersonic expansions.[11,13–19] Though important, these achievements remain insufficient to allow an exhaustive and global modeling of the individual line parameters below 1.7 μm.

This is in particular the case in the important 1.55 μm transparency region which we recently investigated at room temperature by high sensitivity CW-cavity ring down spectroscopy (CRDS).[20] Spectral recordings were then performed with sensitivity corresponding to a noise equivalent absorption of $\alpha_{min} \sim 5 \times 10^{-10}$ cm^{-1}, allowing for the detection of transitions below 10^{-28} cm $molecule^{-1}$, while the weakest lines included in the HITRAN database are around 4×10^{-26} cm $molecule^{-1}$. The spectrum was found to exhibit a highly complex and congested structure with a kind of 'fractal'

[a] *Laboratoire de Spectrométrie Physique (associated with CNRS, UMR 5588), Université Joseph Fourier de Grenoble, B.P. 87, 38402 Saint-Martin-d'Hères Cedex, France. E-mail: Alain.Campargue@ujf-grenoble.fr*
[b] *Hefei National Laboratory for Physical Sciences at Microscale, Department of Chemical Physics, University of Science and Technology of China, Hefei, 230026, China*

† Electronic supplementary information (ESI) available: Movie showing the temperature evolution of the CH_4 spectrum around 6096 cm^{-1} sections during the cooling and warming of the absorption cell down to 80 K. The sample pressure, measured continuously during the cooling, was observed to vary from 1.01 to 0.56 Torr. The displayed spectra correspond to an absorption coefficient normalized at 1 Torr pressure. The insert shows the particular line which was used to determine the temperature at each instant from the fit of its Doppler profile. The fitted Gaussian profile and the residuals are also given in the insert plot. See DOI: 10.1039/b805947k

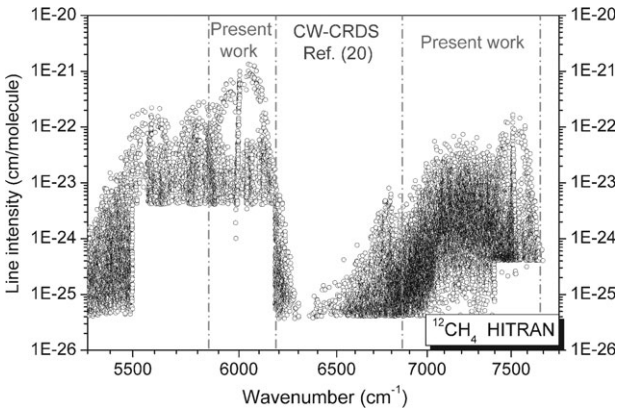

Fig. 1 Overview of the CH_4 spectrum as provided in the HITRAN database for the 5300–7800 cm^{-1} region. The two spectral intervals presently recorded at room temperature and liquid nitrogen temperature by diode laser spectroscopy are indicated. The 1.55 μm transparency window previously recorded by CW-CRDS at room temperature (only) is also indicated.

character and a density of transitions of a few tens per cm^{-1}. In order to contribute to the characterization and rovibrational assignment of the methane absorption spectrum in this 1.55 μm spectral region, we have undertaken the development of a cell cooled at liquid nitrogen temperature in view of future CW-CRDS experiments. In the present report, we describe the first results obtained with this new cell by direct absorption spectroscopy in the strong absorption regions surrounding the above transparency window: the 5850–6190 cm^{-1} region corresponding to the high energy part of the tetradecad and the 6700–7700 cm^{-1} region corresponding to the icosad. The spectral regions of interest are indicated in Fig. 1 which displays the CH_4 spectrum as included in the HITRAN database.

New experimental information relative to these two polyads of interacting vibrational states is expected to help overcoming the analysis difficulties. While the analysis of the first four polyads (up to 4800 cm^{-1}) has been completed by the Dijon's group,[21] the tetradecad and icosad are the next polyads to be modelled at higher energies. Modelling is made extremely difficult by the increasing number of strongly interacting near-degenerate vibration levels: 60 levels for the tetradecad region (5400–6300 cm^{-1}) and 134 levels for the icosad region (6600–7700 cm^{-1}). The additional information contained in spectra recorded at liquid nitrogen temperature (77 K) is expected to be of great benefit for the rovibrational analysis as it will allow (i) reducing the rotational congestion, (ii) resolving a number of multiplets as a consequence of the narrowing by a factor of 2 of the Doppler line width, (iii) determining the lower state J values from the temperature dependence of the line intensities.

After the description of the experimental set up (section 2), spectral data will be presented and analyzed in section 3, which includes a description of the procedure for lower energy level determination from the temperature dependence of line intensities. This method will be illustrated by a continuous monitoring of the spectrum in narrow spectral sections during cool-down of the absorption cell to 77 K or during its warm-up back to room temperature, the measured Doppler broadening being used as an accurate real-time *in situ* thermometer.

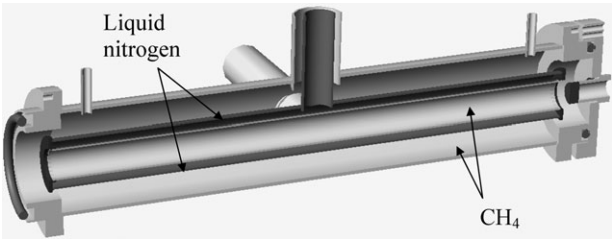

Fig. 2 Schematic diagram of the cell cooled at liquid nitrogen temperature.

2. Experiment

As mentioned above, the cryogenic cell used in the present study was developed for future CW-CRDS recordings in the CH_4 transparency windows. For this reason, a special design (see Fig. 2) was used, different from that of typical cryogenic cells described in the literature. The main point was to avoid internal separation of the cell with a cooled section (cryostat) for the sample, closed by a first pair of windows, itself surrounded by another jacket to be evacuated for thermal insulation, requiring another pair of windows facing the outside world. Double windows are a nuisance for direct absorption spectroscopy as they increase chances of parasitic etaloning effects in the recorded spectra. More importantly, they are incompatible with a CRDS setup where the external windows should be replaced by high reflectivity mirrors. Having windows inside a CRDS cavity introduces optical losses and strongly degrades the cavity finesse. An alternative consists of replacing the internal windows, but this leads to practical complications with respect to the alignment of the optical cavity and especially its stability during temperature changes. Our simple design dispenses with the evacuated volume by exploiting the fact that we want to perform high resolution spectroscopy with a low pressure sample, which itself may constitute a good thermal insulation. We eliminate the internal pair of windows so the sample fills both the inside of the cryostat and the thermal insulation volume. The cryostat is now completely suspended inside the sample volume through its liquid nitrogen filling tube, which eliminates stresses normally present in a double-jacket cell configuration. Inside the cryostat, which has the shape of a long hollow cylinder, the sample should rapidly equilibrate to its temperature. Given that gas density (at constant pressure) is inversely proportional to temperature, colder gas would be expected to spill out of the cold channel through its extremities and fall down, while being replaced by warm gas, resulting in a convective motion. However, at low pressure gas dynamics become dominated by diffusion and the net result is not so evident without further investigation. We decided to take a pragmatic approach and test this simple cell configuration with direct absorption measurements.

We will give here more details about the cell. The external stainless steel cylinder is 1.4 m long, with a diameter of Φ = 6.3 cm, while the cryostat is made of two co-axial tubes

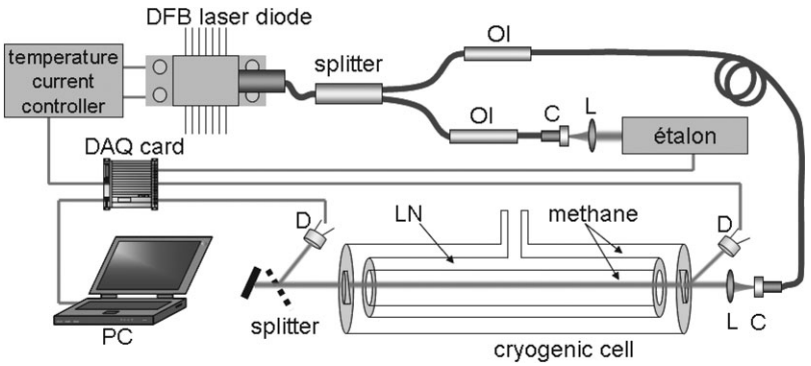

Fig. 3 Scheme of the experimental arrangement for the absorption spectroscopy of methane cooled by liquid nitrogen. OI: optical isolator, C: fiber coupler, L: lens, D: detector, LN: liquid nitrogen.

(Φ = 1.6 and 2 cm) joined at the ends by two rings and suspended at the center by a 2 cm in diameter tube used for filling the cryostat. For the present direct absorption experiments, the distance between the windows and the cryostat ends is 1 cm. For pressures below 10 Torr, heat transfer is slow and insufficient to cool significantly the external walls, even after several hours of operation. Only the windows showed significant cooling eventually leading to water condensation, which was avoided by blowing dry air onto them.

Spectra were recorded by direct absorption spectroscopy using a series of DFB fibered diode lasers as a light source (most of them were 20 mW butterfly mounted, by NEL) allowing a continuous coverage of the large 1.27–1.7 μm spectral range. For this study 15 and 35 DFB diodes were necessary to record the spectra in the 5960–6170 cm^{-1} and 6700–7680 cm^{-1} region, respectively.

Fig. 3 shows the schematic of the experimental arrangement. A 50/50 fibered beam splitter drives part of the laser light to a home-made étalon (BK7 glass, 10 cm length), while the other fraction is sent through the absorption cell sealed by two wedged anti-reflection coated windows. The weak beam reflected from the input cell window is used as reference while a third window (same type as the others) picks up part of the transmitted light. This arrangement ensures the signal and reference beams have similar intensities thus allowing the use of two identical photodetectors (InGaAs photodiodes with home-made transimpedance amplifiers). A multifunction DAQ card (NI-USB-6251) was used to control the laser temperature by providing a voltage setpoint to a homemade fast temperature controller, while acquiring the photodiode signals (étalon, reference and transmission) at a rate of 400 kHz.

While a fast periodic current ramp (16 ms) opens a 1 cm^{-1} wide window, a slow temperature scan at about 6 °C min^{-1} sweeps this window over a whole DFB tuning range of about 30 cm^{-1} within 12 min. The étalon trace allows the 1 cm^{-1} spectral scans to be unambiguously and dynamically overlapped and averaged to produce the final complete spectrum for a given laser diode. The spectral points, each resulting from the averaging of about 100 acquisitions, are at 10 MHz intervals, about 50 times below the Doppler width (HWHM) of CH_4 at room temperature.

In summary, each complete diode laser spectrum consists of the dynamic averaging and concatenation of several thousands smaller spectra (1 cm^{-1} wide) obtained by a fast current ramping with a 10 MHz spectral resolution. These 30 cm^{-1} wide spectra were calibrated independently by matching accurate CH_4 line positions measured by FTS at room temperature[2] and adopted in the HITRAN database. The standard deviation error of the differences between our line positions and HITRAN values was minimized (rms values are less than 10^{-3} cm^{-1}).

The typical achieved noise equivalent absorption is 2×10^{-6} cm^{-1} corresponding to a detection limit on the order of 10^{-25} cm $molecule^{-1}$ for the line intensities at room temperature with a pressure of 10 Torr. The gas pressure as measured by a capacitance gauge (MKS Baratron, 10 Torr range) was continuously recorded during the spectrum acquisition.

3. Results and discussion

Temperature and line intensity retrievals

Several series of recordings were performed at pressure ranging from 1.0 to 12 Torr. For the sake of simplicity, we focus below mostly on the analysis of spectra recorded at low pressure. In these pressure conditions, the collisional broadening ($\sim 9.0 \times 10^{-5}$ cm^{-1} HWHM at 1.0 Torr[2] at room temperature) is significantly smaller than the Doppler width (HWHM 9.5×10^{-3} cm^{-1} at room temperature). As the DFB laser line width is negligible (a few MHz), the observed line profile is mostly a Gaussian profile. The integrated absorbance, I_{ν_o}, (in cm^{-2} $molecule^{-1}$) and the half width at half maximum (HWHM) were obtained for each line using an interactive least squares multi-lines fitting program. The first (manual) step of the analysis consisted in the determination of the spectral sections consisting of overlapping transitions that could then be fitted independently. The position, HWHM and integrated absorbance of each line together with a baseline (assumed to be a second order polynomial function of the wavenumber) were provided by the fitting procedure. The gas temperature was then obtained directly from the Doppler HWHM, ν_D, using the standard expression:

$$\nu_D = \frac{\nu_0}{c}\sqrt{\frac{2kT}{M}\ln 2} \qquad (1)$$

where ν_0 is the line centre in cm^{-1}, T is the temperature, M is the molecular mass and k is the Boltzmann constant. Fig. 4

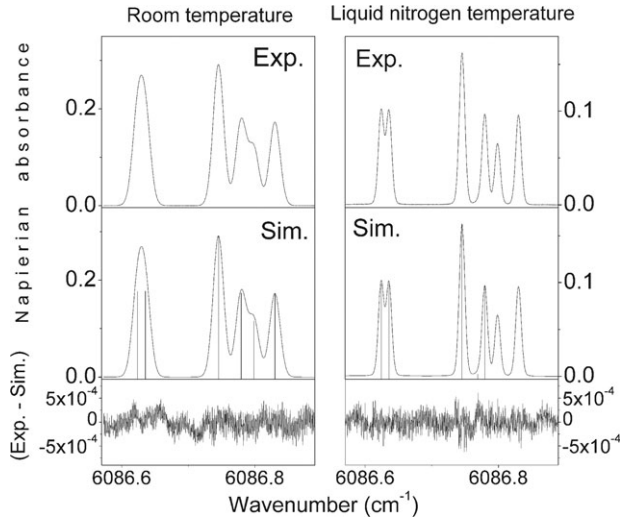

Fig. 4 Comparison of the CH_4 spectrum recorded at room temperature (left hand) and liquid nitrogen temperature (right hand) with its simulation assuming the same profile for the different lines: (a) experimental spectrum; (b) simulated spectrum resulting from the fitting procedure (see text); (c) residuals between the simulated and experimental spectra. The pressure values were 0.71 and 1.22 Torr for the RT and LNT spectra, respectively.

shows a comparison between the measured and fitted spectra recorded at room temperature (RT) and at liquid nitrogen temperature (LNT). The high signal to noise ratio of the spectra allowed decreasing to a very small value (about 2×10^{-4}) the rms of the residuals of the simulation. The pressure values were 0.71 and 1.22 Torr for the RT and LNT spectra, respectively. In the simulation of the RT spectrum, the same Gaussian Doppler profile was affected to each line and the obtained room temperature was 295 K. In the simulation of the LNT spectrum, a similar simulation led to a temperature value of 82.5 K and an rms value of the residuals of about 4×10^{-4}. This rms value could be further decreased by a factor of two using a Voigt profile but the Gaussian component corresponded to a 75 K gas temperature. It is not clear whether the Lorentzian component (with a width of about half the Gaussian width) is an effective profile due to the small sections of warm gas lying between the ends of the cold jacket and the cell windows or if a more sophisticated velocity dependent profile should be used to reproduce the observed line profile. Let us underline that the observation of these small effects is a consequence of the high signal to noise ratio of the spectrum. The effect of the non-uniformity of the temperature all over the cell axis is in fact reduced by the higher density of the colder gas. It would be interesting to check if the evidenced deviation from a Gaussian profile is more pronounced for the transitions corresponding to high rotational energy levels which are expected to be more affected by the warm gas sections.

Some characteristics of the low temperature spectra

The LNT and RT spectra in the region of the Q branch of the $2\nu_3$ band, which dominates the tetradecad, is presented in Fig. 5. The depletion of the population corresponding to high J rotational levels is clearly reflected by the reduction of the

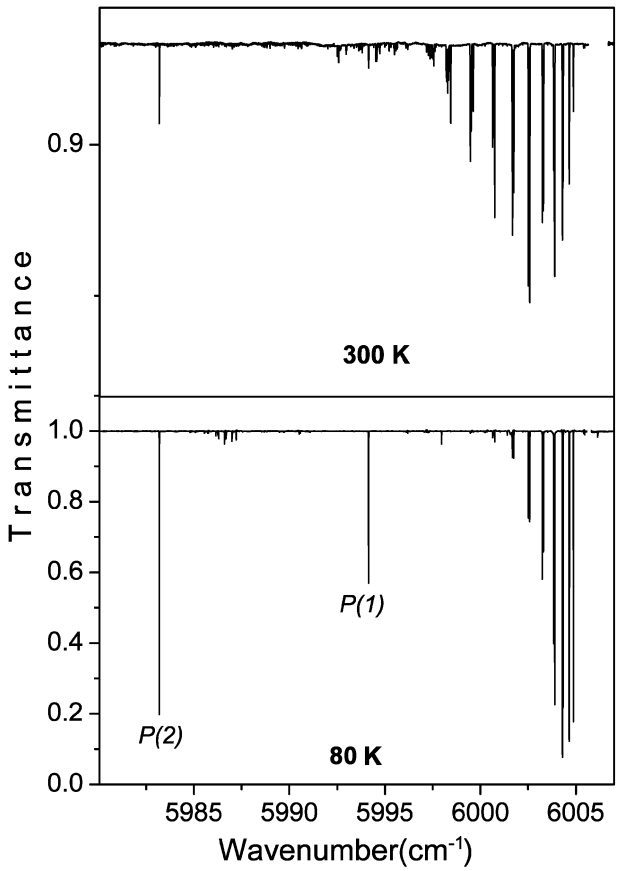

Fig. 5 The liquid nitrogen and room temperature spectra of methane in the region of the Q branch of the $2\nu_3$ band which dominates the tetradecad. The room temperature and cold spectra were recorded at 1.0 and 0.75 Torr, respectively. Note the reduction of the extension of the Q branch and the strong increase of the intensity of the $P(1)$ and $P(2)$ lines in the LNT spectrum.

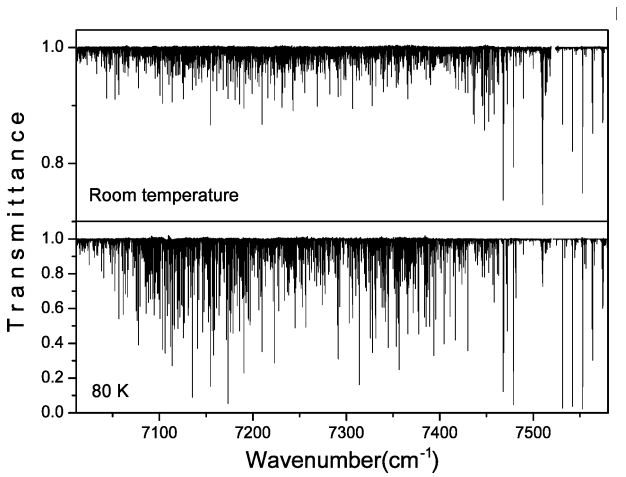

Fig. 6 Overview of the liquid nitrogen and room temperature spectra of methane in the region of the icosad (7000–7600 cm^{-1}). The room temperature and cold spectra were recorded at 11.8 and 9.7 Torr, respectively (see comments in the text). Note the change in the ordinate scale.

extension of the Q branch and the $P(1)$ and $P(2)$ line intensities increase considerably. The overview of the spectrum in the icosad region (Fig. 6) shows an extremely complex and dense structure even at 80 K. The reduction of the rotational congestion is not visually apparent on this graph. This is due to the fact that the two displayed spectra were recorded with similar sample pressure and the molecular concentration was about four times larger for the low temperature spectrum. The increase of the peak depth (by a factor of about 2) due to the line narrowing at low temperature also contributes to the apparent increase of the absorption lines in the low temperature spectrum, independently of the variation of the line intensities during the cooling.

Fig. 7 and 8 show a sequence of spectra recorded during the cooling of the cell, just after filling the cryogenic tank with liquid nitrogen. The displayed spectra correspond to two 1 cm^{-1} wide sections of the tetradecad. The temperature calculated from the Doppler line broadening decreased from room temperature down to 80 K within about 20 min. Even more illustrative is the short movie attached as ESI† which allows following continuously the spectrum evolution with temperature. The change in the intensity distribution is so considerable that in some spectral regions, the same spectra recorded at LNT and RT are hardly recognizable (see the upper and lower panels of Fig. 7 and 8). Of importance for the spectral analysis is the reduction by a factor of 2 of the Doppler line width allowing for the resolution of a number of multiplets which are strongly blended at room temperature.

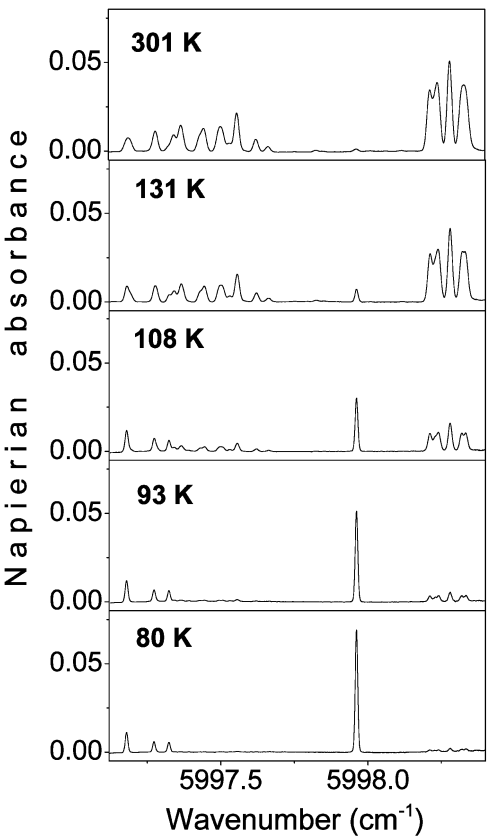

Fig. 7 Temperature evolution of the methane absorption spectrum near 5998 cm^{-1}. The strong line dominating the spectrum at 80 K is the $R(0)$ transition of the $2\nu_3$ band of $^{13}CH_4$ present in natural abundance in the sample.

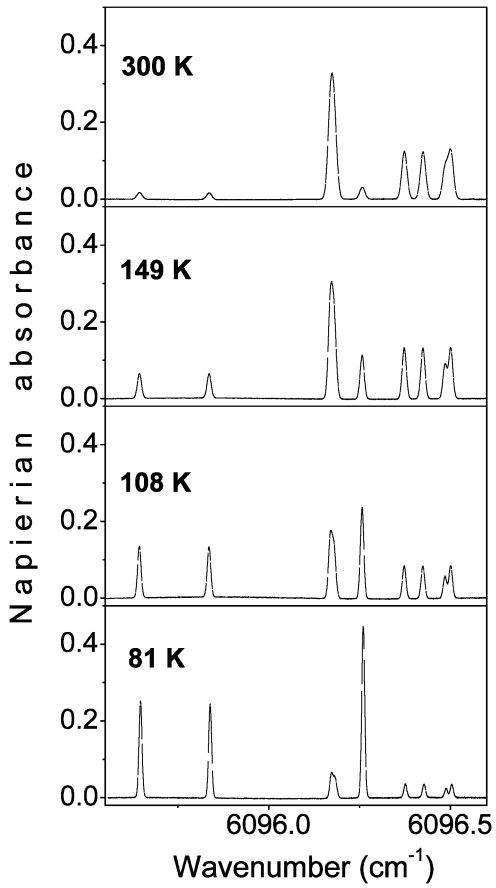

Fig. 8 Temperature evolution of the methane absorption spectrum near 6096 cm^{-1}. The intensity variation allows to discriminate two groups of lines: the three stronger lines in the 81 K spectrum arise from $J = 3$ levels while the others correspond to $J = 8$ (see also Fig. 7 and 8).

Determination of the lower state energy

The low energy value, E'', and then the value of J'' as $E'' \approx B_0 J''(J'' + 1)$, can be deduced from the intensity value of a given line recorded at two temperatures. This is true independently of any rovibrational assignment as long as individual line intensities can be accurately determined.

The integrated line absorbance, I_{ν_0}, of a rovibrational transition centred at ν_0, can be expressed as:

$$I_{\nu_0}(T) = \int_{\text{line}} \alpha_\nu \, l \, d\nu = \int_{\text{line}} \ln\left[\frac{I_0(\nu)}{I(\nu)}\right] d\nu = S_{\nu_0}(T) N l \quad (2)$$

where $\frac{I_0(\nu)}{I(\nu)}$ is the ratio of the incident intensity over the transmitted intensity, S_{ν_0} is the line intensity in cm $molecule^{-1}$, l is the absorption pathlength in cm, ν is the wavenumber in cm^{-1}, $\alpha(\nu)$ is the absorption coefficient in cm^{-1}, N is the molecular concentration in molecule cm^{-3}.

The dependence of line intensity *versus* temperature is as follows:

$$S_{v_0}(T) = S_{v_0}(T_0)\frac{Q(T_0)}{Q(T)}\exp\left[-E''\left(\frac{1}{kT}-\frac{1}{kT_0}\right)\right] \quad (3)$$

where T_0 is a reference temperature and $Q(T)$ is the internal partition function. Note that the extremely weak stimulated emission term from the upper level of the transition is neglected. As the energies of the excited vibrational states are very high compared to the considered thermal energies, the vibrational contribution to the partition function is also negligible and only the rotational partition sum has to be considered:

$$\frac{Q(T_0)}{Q(T)} = \left(\frac{T_0}{T}\right)^{3/2} \quad (4)$$

Taking into account the temperature dependence of the molecular density:

$$N = \frac{P}{kT}, \quad (5)$$

we derive the following dependence of the integrated line absorbance as a function of temperature and pressure:

$$\begin{aligned} I_{v_0}(T) &= S_{v_0}(T)Nl \\ &= S_{v_0}(T_0)\left(\frac{T_0}{T}\right)^{3/2}\exp\left[-E''\left(\frac{1}{kT}-\frac{1}{kT_0}\right)\right]\frac{Pl}{kT} \quad (6) \\ &\propto PT^{-5/2}\exp\left[-\frac{E''}{kT}\right] \end{aligned}$$

The integrated absorbance normalized to pressure is then simply related to temperature:

$$\frac{I_{v_0}(T)}{P} \propto T^{-5/2}\exp\left[-\frac{E''}{kT}\right] \quad (7)$$

The pressure being continuously monitored during the recordings, the quantity $\frac{I_{v_0}(T)}{P}$ is experimentally known. The dependence of the quantity $-\ln\left[\frac{I_{v_0}(T)T^{5/2}}{P}\right]$ *versus* $\frac{1}{kT}$ is then expected to be linear with a slope equal to the lower energy level of the considered transition. The continuous recording of spectral evolution during the cooling gives a unique opportunity to check this dependence. Fig. 9 shows the plot relative to eight lines around 6096 cm^{-1} observed in the sequence of Fig. 8. The slopes of the obtained temperature dependence allow discriminating two groups of lines: 3 transitions corresponding to the energy value of the $J = 3$ lower level (62.88 cm^{-1})[22] and 5 transitions corresponding to the energy value of the $J = 8$ lower level (376.8 cm^{-1}).[22] It is important to note that in the case of methane, the rotational constant B_0 is large (5.24 cm^{-1}) which leads to an important gap between the energy value of two successive J levels and helps obtain an unambiguous J assignment. A comparison of the slopes associated with two particular lines with the $J = 0$–11 theoretical slopes (Fig. 10) leaves no doubt about their J assignment. Considering that, for a given J value, the tetrahedral splitting is small (less than 0.25 cm^{-1} at $J = 10$),[22] the uncertainty on the low energy value is in fact much smaller than the uncertainty derived from the experimental slopes.

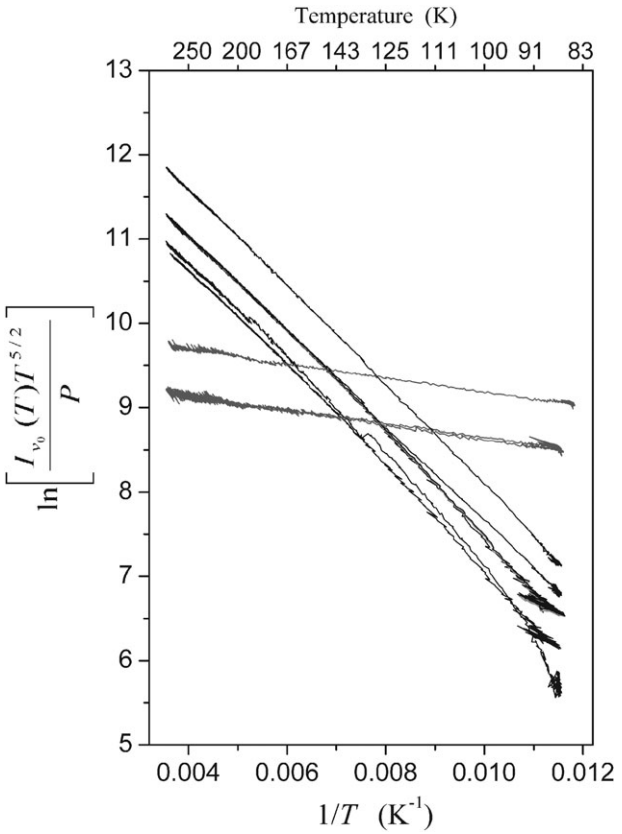

Fig. 9 Variation of the quantity $\ln\left[\frac{I_{v_0}(T)T^{5/2}}{P}\right]$ *versus* $\frac{1}{kT}$ during the warming of the gas sample from 80 K to room temperature, for the nine CH_4 lines around 6096 cm^{-1} observed in Fig. 6.

The plot displayed in Fig. 9 was actually obtained during the warming of the cell from liquid nitrogen to room temperature. We noted that the warming being more progressive (typically 2 h) than the cooling (typically 20 min), more consistent results could be obtained as the gas temperature is more uniform all along the inner part of the cryogenic chamber.

Application to the 6092–6124 cm^{-1} region

The above lower energy determination from the retrieval of the line intensities all along the cooling or warming phases is excessively time consuming to be applied to extended spectral ranges. Nevertheless, the above results provide a convincing validation of the method.

In principle, the determination of the lower state energy from the dependence of the line intensities requires only two spectra recorded at different temperatures (see eqn (7)). Among the experimental investigations of the absorption spectrum of CH_4 in a cell cooled at low temperature,[5–12] two studies used this method: Pierre *et al.*[8] determined lower state quantum numbers in the region of the $3\nu_3$ band near 9000 cm^{-1} from spectra recorded at 295 and 149 K by Fourier transform spectroscopy with a white cell (80 cm base length and 51 m path length) while Tsukamuto *et al.*[9] could

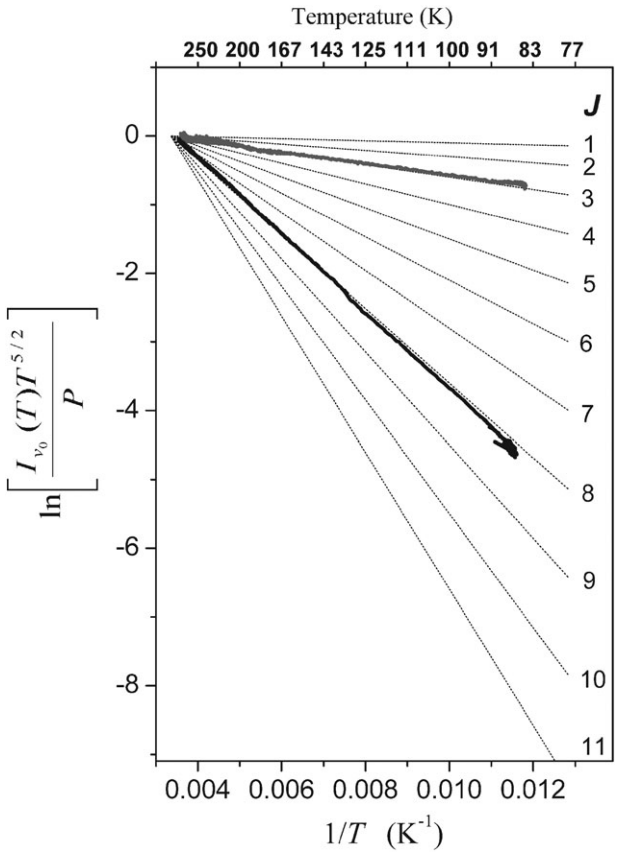

Fig. 10 Discrimination of the J value of the low energy level from the slope of the variation of the quantity $\ln\left[\frac{I_{v_0}(T)T^{5/2}}{P}\right]$ *versus* $\frac{1}{kT}$ during the warming of the gas sample from 80 K to room temperature: the comparison of the experimental slope corresponding to the transition lines centered at 6095.6401 and 6096.3726 cm^{-1} with the theoretical[22] slope corresponding to $J = 0$–11 values leaves no doubt about their J assignment to $J = 3$ and $J = 8$, respectively. Note that the straight lines associated to the experimental values have been vertically translated in order to coincide at room temperature and make the comparison easier.

tentatively assign 215 transitions with respect to J'' among the 269 transitions of the $3\nu_1 + \nu_3$ that they recorded by tone-burst modulation spectroscopy at 77 K. As a further example, we applied the same method to all the lines detected over a 30 cm^{-1} section of the spectrum corresponding to the full tuning range of one DFB laser diode (6092.2–6123.8 cm^{-1}). The centre, HWHM and absolute line intensity of 128 lines were obtained by line fitting of the spectra at low temperature. The chosen spectrum was recorded at 0.75 Torr, and a purely Gaussian profile was assumed. Fig. 11 shows the small dispersion of the temperature values calculated from the HWHM values. An average value of 81.2 ± 2.1 K is obtained without excluding any outlier, the error bar corresponding to one standard deviation. If, among the 128 temperature values, we exclude 14 outliers due to weak or blended lines, we obtain an average value of 81.8 ± 0.7 K. The obtained accuracy values show that the measurement from Doppler line broadening is a very precise way to measure the gas temperature in a cooled cell.

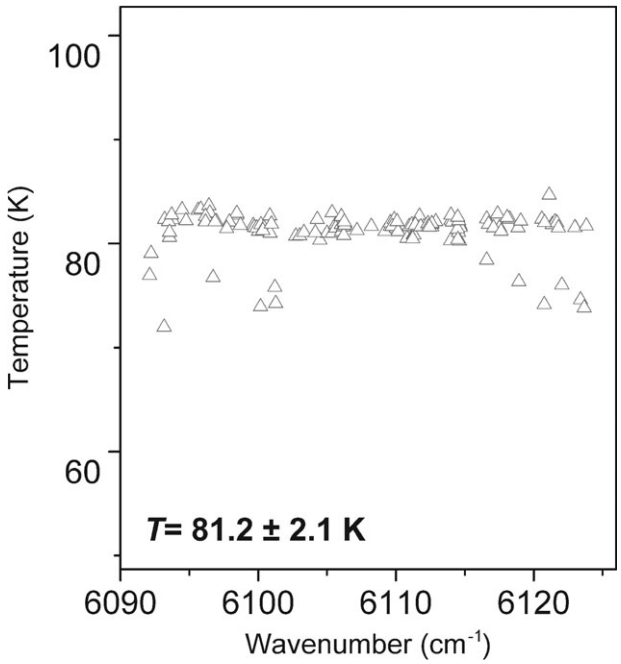

Fig. 11 Scattered graph, *versus* the line centre, of the temperature values calculated from the HWHM values of the 126 transitions observed in the low temperature spectrum of CH_4 between 6093 and 6124 cm^{-1}.

For the room temperature line intensities, we adopted the accurate values of the 107 transitions provided by the HITRAN database[2] in the considered spectral region. 54 of these lines are in coincidence with our low temperature line list. Table 1 lists the whole set of transitions measured at low temperature with their corresponding intensity at 80 K and also at 296 K when available in HITRAN. Following eqn (7), the lower state energy was obtained for the lines present in the two data sets:

$$\left[\ln\left[\frac{I_{v_0}(T)T^{5/2}}{P}\right]\right]_{T=80}^{T=296} = -E''\left[\frac{1}{kT}\right]_{T=80}^{T=296} \qquad (8)$$

We present in Fig. 12 a scattered graph of the obtained E'' values *versus* the line centre. The well known values of the lower energy rotational levels[22] are indicated on this graph together with their corresponding J value. The nice agreement between the obtained and expected E'' values leaves no doubt for the assignment of the transitions with J'' value up to 10. Overall, about half of the common lines can be unambiguously J assigned. The J assignments, obtained as the positive root of the $E'' = B_0J''(J'' + 1)$ equation, are included in Table 1. The agreement degrades for higher J values due to the weakness of the corresponding transitions in the low temperature spectrum. We have already recorded low temperature spectra with a ten times higher pressure (about 7 Torr) whose analysis will allow extending to higher J values the set of unambiguously assigned transitions. To a lesser extent, a similar limitation is found for the $J = 0$–2 values which are weak lines partly absent in the HITRAN database due to the fact the HITRAN intensity cut off in the considered region was fixed to a relatively high value (4×10^{-24} cm $molecule^{-1}$). However, the steep increase of the line intensities of the $J = 0$–2

Table 1 Line positions and absolute line intensities of the transitions observed in the CH_4 absorption spectrum recorded at 81 K with a 0.70 Torr pressure. The J value of the low energy level (last column) was determined for 54 transitions using the intensity value at 296 K as provided by the HITRAN database (third column)[a]

Line center/cm^{-1}	Line intensity/10^{-24} cm mol^{-1} T = 81 K, This work	T = 296 K[2]	J_{low}
6092.1226	0.89		
6092.2251	4.25		
6093.1694	2.16		
6093.2056	21.84	12.65	4.0
6093.4888	12.36	6.82	3.9
6093.5679	8.07		
6093.5684	3.70		
6093.7163	7.62		
6093.7749	13.12	7.35	4.0
6094.4736	19.67	11.23	4.0
6094.7656	1.82		
6095.6401	151.12	48.37	2.9
6095.8330	148.00		
6096.1680	37.00	538.30	7.8
6096.1763	22.89	718.40	8.5
6096.1812	15.78	326.80	8.1
6096.2563	269.49	86.92	2.9
6096.3726	21.87	455.30	8.4
6096.4243	21.67	453.30	8.4
6096.4858	14.47	312.70	8.3
6096.5015	21.43	440.20	8.3
6096.7217	1.04		
6096.8652	0.94		
6096.9673	1.07		
6097.7217	0.68		
6097.9063	9.49		
6098.4487	133.00		
6098.4639	201.00		
6098.7134	2.24		
6099.6450	2.32		
6099.7129	1.88		
6099.8945	1.04		
6100.0278	1.00		
6100.1675	2.03		
6100.2007	12.30		
6100.3423	0.44	28.84	9.1
6100.4121	1.09		
6100.8477	0.87	58.99	9.1
6100.8613	10.10		
6100.9575	0.54	32.38	9.0
6101.2153	1.33		
6101.2710	2.29		
6102.7280	16.35	19.02	5.1
6103.0254	8.53	10.32	5.1
6103.3149	10.39	12.55	5.1
6104.1470	0.77		
6104.2871	7.67		
6104.4834	0.72		
6104.9922	11.10		
6105.3662	9.91		
6105.3745	12.80		
6105.6250	3.19		
6105.6250	6.93		
6105.6279	3.92		
6106.0371	145.00		
6106.0454	8.17		
6106.0537	79.40		
6106.1953	79.62	46.44	4.0
6106.2217	3.90	284.30	9.2
6106.2529	3.76	300.50	9.2
6106.2852	7.16	513.00	9.1
6106.3003	86.50		
6107.1689	86.47	49.38	4.0
6108.2109	2.87		
6109.2065	5.13		
6109.5942	0.50		
6109.6064	118.00		
6109.7236	117.54	37.74	2.9
6109.8838	130.97	42.60	3.0
6110.0381	257.74	84.29	3.0
6110.0791	18.13		
6110.1548	1.28		
6110.8130	1.11		
6110.9658	3.37		
6111.1616	0.48		
6111.2158	1.69		
6111.2598	1.10		
6111.2979	0.58		
6111.4058	0.71		
6111.7114	18.20		
6111.8018	18.13	6.00	3.0
6112.0205	16.81	47.66	6.2
6112.3262	3.34		
6112.3486	0.65		
6112.4360	5.95		
6112.5918	5.70	25.30	6.7
6112.5986	1.02		
6112.6128	9.15		
6112.8940	9.20	24.59	6.1
6113.9729	3.40		
6113.9937	3.44	9.92	6.3
6114.0010	2.63		
6114.0840	1.65		
6114.4805	1.17	342.00	10.2
6114.4893	1.99		
6114.4995	1.58	384.50	10.1
6114.5498	0.63	132.60	9.9
6114.5625	0.43	67.49	9.8
6114.6025	0.24	16.80	9.1
6114.6143	0.54	157.90	10.2
6114.6646	2.06	486.70	10.0
6114.6768	1.98	454.30	10.0
6116.5928	35.23	41.28	5.1
6116.5939	3.06		
6116.7236	33.05	38.45	5.1
6117.0815	24.15		
6117.3862	3.32		
6117.5313	24.40		
6117.6333	35.60		
6118.0801	0.51		
6118.2573	35.45	41.79	5.1
6118.8701	1.55		
6118.9297	1.30	9.84	7.1
6119.0547	0.96		
6120.5869	88.15	52.21	4.1
6120.7749	61.60		
6120.7896	44.70		
6121.1304	61.37	35.62	4.0
6121.3535	44.64	25.70	4.0
6121.5459	3.84	26.61	7.3
6121.6826	85.63	48.97	4.0
6121.8018	2.19	15.79	7.2
6122.0537	2.40	17.61	7.2
6123.0020	1.01	98.25	9.4
6123.0127	1.07		
6123.4063	3.25	27.22	7.3
6123.6626	1.07		
6123.8247	1.53		

[a] The listed HITRAN values correspond to pure $^{12}CH_4$.

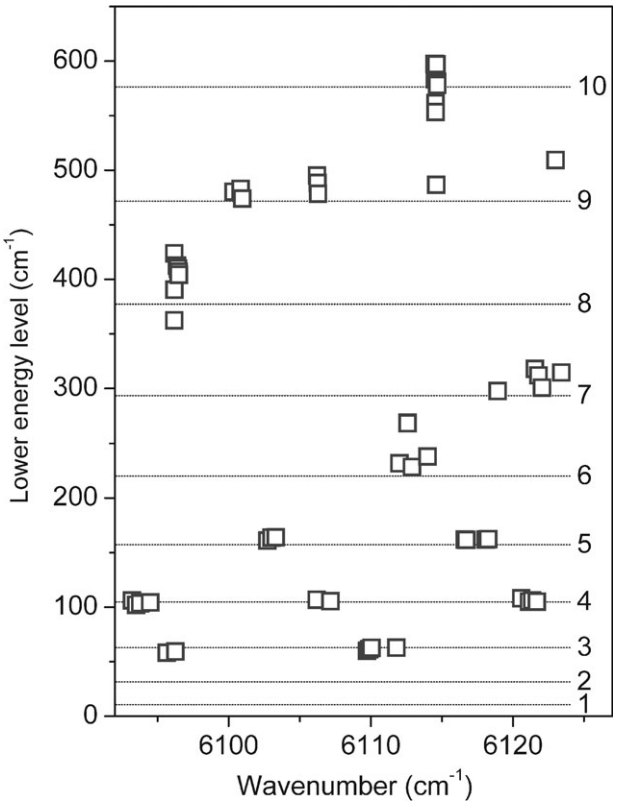

Fig. 12 Scattered graph of the lower energy values, E'', obtained from the analysis of the methane spectrum recorded at 80 and 300 K between 6093 and 6124 cm^{-1}, *versus* the line centre. The graph corresponds to the 54 transitions present in both our 80 K line list and HITRAN (296 K). The values of the lower energy rotational levels[22] are indicated together with their corresponding J values.

transitions in the 80 K spectrum is a clear signature of these low J levels (see Fig. 5 and 7). If necessary, additional recordings at an intermediate temperature and/or with a more sensitive experimental method could be considered in order to further increase the number of unambiguous assignments. An alternative solution in specific spectral regions would be the continuous spectrum monitoring during the cooling or warming of the cell as presented above.

4. Conclusion

We have developed and tested a simple and original design for a cryogenic cell without external vacuum jacket for absorption spectroscopy experiments, which we hope will prove to work also with CRDS, where the cell windows will be replaced by high reflectivity mirrors. In the present work, this cell was used for recording the high resolution spectrum of methane cooled at 80 K by direct absorption spectroscopy between 1.30 and 1.70 μm. The typical noise equivalent absorption was 2×10^{-6} cm^{-1} which corresponds to a detection threshold on the order of 10^{-25} cm $molecule^{-1}$ for the line intensities (at 300 K and with a 10 Torr pressure). The reduction of the rotational congestion and the line width narrowing at low temperature will help future rovibrational modeling of the spectrum in the tetradecad and icosad regions. The measured Doppler line broadening was found to be a reliable method for determining the gas temperature as long as the line profile can be approximated by a Gaussian function. This method is an interesting alternative to the usual temperature determination from the rotational intensity distribution. It has the advantage of not requiring any rotational assignment and the accuracy of the obtained average temperature value can be improved by the statistics over a large number of analyzed transitions. A short movie illustrating the temperature evolution of methane absorption in a selected spectral region during the cooling and warming of the cell is attached as ESI.† To our knowledge, it is the first time that line intensities could be continuously measured from room temperature down to 77 K.

This method validated a procedure for the retrieval of the J rotational assignment of the lower level from the temperature variation of the absolute line intensities. It has been applied to 54 transitions detected in a 30 cm^{-1} section of the tetradecad around 6110 cm^{-1}. We are planning to apply this approach to the whole spectral region where we recorded two series of spectra (80 and 300 K) at different pressures. Considering the spectral congestion and the number of spectra, data analysis will be a considerable task. However, the obtained values of the low energy level will allow simulating the methane spectrum at any intermediate temperature between 80 and 300 K, independently of any rovibrational Hamiltonian modeling. The quality of the simulation will benefit from the fact that, once the J assignment has been obtained, the uncertainty on the low energy value is fixed by the corresponding tetrahedral splitting which is limited to a few tenths of wavenumber up to $J = 12$.[22] We believe these results will contribute to a better characterization and modeling of methane absorption in spectral regions which are of primary importance in planetology.

Note added in proof

After the acceptance of our paper, we have become aware of the previous study of Margolis[23] which is of particular relevance for the present study. The low energy values derived in the present work are in good agreement with Margolis' results. In a future contribution, these previous results will be compared and discussed in detail.

Acknowledgements

This work is supported by the Programme National de Planétologie (CNRS, INSU) and a collaborative project between CNRS and CAS-China (PICS grant No 3359). S. Béguier (LSP) is warmly acknowledged for his contribution to the line fitting analysis.

References

1. V. Boudon, M. Rey and M. Loëte, *J. Quant. Spectrosc. Radiat. Transfer*, 2006, **98**, 394–404.
2. L. S. Rothman, D. Jacquemart, A. Barbe, D. C. Benner, M. Birk, L. R. Brown, M. R. Carleer, C. Chackerian, Jr, K. Chance, L. H. Coudert, V. Dana, V. Malathy Devi, J.-M. Flaud, R. R. Gamache, A. Goldman, J.-M. Hartmann, K. W. Jucks, A. G. Maki, J.-Y. Mandin, S. T. Massie, J. Orphal, A. Perrin, C. P. Rinsland, M. A. H. Smith, J. Tennyson, R. N. Tolchenov,

J. Vander Auwera, P. Varanasi and G. Wagner, *J. Quant. Spectrosc. Radiat. Transfer*, 2005, **96**, 139–204.
3. N. Jacquinet-Husson, N. A. Scott, A. Chédin, K. Garceran, R. Armante, A. A. Chursin, A. Barbe, M. Birk, L. R. Brown, C. Camy-Peyret, C. Claveau, C. Clerbaux, P. F. Coheur, V. Dana, L. Daumont, M. R. Debacker-Barilly, J. M. Flaud, A. Goldman, A. Hamdouni, M. Hess, D. Jacquemart, P. Kopke, J. Y. Mandin, S. Massie, S. Mikhailenko, V. Nemtchinov, A. Nikitin, D. Newnham, A. Perrin, V. I. Perevalov, L. Régalia-Jarlot, A. Rublev, F. Schreier, I. Schult, K. M. Smith, S. A. Tashkun, J. L. Teffo, R. A. Toth, Vl. G. Tyuterev, J. Vander Auwera, P. Varanasi and G. Wagner, *J. Quant. Spectrosc. Radiat. Transfer*, 2005, **95**, 429–467.
4. L. Brown, *J. Quant. Spectrosc. Radiat. Transfer*, 2005, **96**, 251–270.
5. G. J. Scherer, K. K. Lehmann and W. Klemperer, *J. Chem. Phys.*, 1984, **81**, 5319–5325.
6. J. J. O'Brien and H. Cao, *J. Quant. Spectrosc. Radiat. Transfer*, 2002, **75**, 323–350.
7. K. Singh and J. J. O'Brien, *J. Quant. Spectrosc. Radiat. Transfer*, 1995, **54**, 607–619.
8. G. Pierre, J.-C. Hilico, C. de Bergh and J.-P. Maillard, *J. Mol. Spectrosc.*, 1980, **82**, 379–393.
9. T. Tsukamoto and H. Sasada, *J. Chem. Phys.*, 1995, **102**, 5126–5325.
10. A. R. W. McKellar, *Can. J. Phys.*, 1989, **67**, 1027–1035.
11. K. Boraas, D. Deboer, Z. Lin and J. P. Reilly, *J. Chem. Phys.*, 1993, **99**, 1429–1432.
12. M. W. Crofton, C. G. Stevens, D. Klenerman, J. H. Gutow and R. N. Zare, *J. Chem. Phys.*, 1988, **89**, 7100–7111.
13. A. Campargue, M. Chenevier and F. Stoeckel, *Chem. Phys. Lett.*, 1991, **183**, 153–157.
14. A. Campargue, D. Permogorov and R. Jost, *J. Chem. Phys.*, 1995, **102**, 5910–5916.
15. M. Hippler and M. Quack, *Chem. Phys. Lett.*, 1999, **314**, 273–28.
16. M. Hippler and M. Quack, *J. Chem. Phys.*, 2002, **116**, 6045–6055.
17. A. Amrein, M. Quack and U. Schmitt, *J. Phys. Chem.*, 1988, **92**, 5455–5466.
18. K. Boraas, D. Deboer, Z. Lin and J. P. Reilly, *J. Chem. Phys.*, 1994, **100**, 7916–7927.
19. O. Votava, M. Masat and P. Pracna, Poster L4, HRMS, 20th Colloquium, Dijon, France, September 3–7, 2007.
20. A. W. Liu, S. Kassi and A. Campargue, *Chem. Phys. Lett.*, 2007, **447**, 16–20.
21. J.-C. Hilico, O. Robert, M. Loëte, S. Toumi, A. S. Pine and L. R. Brown, *J. Mol. Spectrosc.*, 2001, **208**, 1–13.
22. J.-P. Champion, J.-C. Hilico and L. R. Brown, *J. Mol. Spectrosc.*, 1989, **133**, 244–255.
23. J. S. Margolis, *Appl. Opt.*, 1990, **29**, 2295–2302.